

## How Bursty is Star Formation at $z > 5$ ?

MASSIMO STIAVELLI<sup>1,2</sup> AND MASSIMO RICOTTI<sup>3</sup>

<sup>1</sup>Space Telescope Science Institute, 3700 San Martin Drive, Baltimore, MD 21218, USA

<sup>2</sup>Dept. of Physics & Astronomy, Johns Hopkins University, Baltimore, MD 21218, USA

<sup>3</sup>Dept. of Astronomy, University of Maryland, College Park, MD 20742, USA

### Abstract

Motivated by observational evidence from JWST and theoretical results from cosmological simulations, we use a simple parametric, phenomenological model to test to what extent bursty star formation with standard Initial Mass Function, no continuous star formation, no mergers, can account for the observed properties in the  $M_{UV}$  vs  $M_*$  plane of galaxies at redshifts  $z > 5$ . We find that the simplest model that fits the data has a quiescence period between bursts  $\Delta t \sim 100$  Myrs and the stellar mass in each galaxy grows linearly as a function of time from  $z = 12$  to  $z = 5$  (i.e., repeated bursts in each galaxy produce approximately equal mass in stars). The distribution of burst masses across different galaxies follows a power-law  $dN/dM_* \propto M_*^\alpha$  with slope  $\alpha \sim -2$ . At  $z > 9 - 10$  the observed galaxy population typically had only one or two bursts of stars formation, hence the observed stellar masses at these redshifts (reaching  $M_* \sim 10^{10} M_\odot$ ), roughly represent the distribution of masses formed in one burst.

### 1. INTRODUCTION

With the advent of JWST evidence for a major role of bursty star formation in high redshift galaxies has gone up considerably, *e.g.* Adamo et al. (2024). There is also evidence that the starburst and *normal* galaxy tracks merge together at high redshift and low galactic masses, *e.g.* Caputi et al. (2024), Rinaldi et al. (2024). Numerical simulations also provide support to the idea of bursty star formation as shown, *e.g.*, by Sugimura et al. (2024); Pallottini et al. (2024); Garcia et al. (2025). It should be noted that other groups have modelled stochastic or bursty star formation with different results.

On the basis of this evidence and these results, we have asked ourselves whether the entirety of star formation in low-mass galaxies could be happening in bursts without any significant continuous star formation, mergers, . If such a simple model can reproduce the observations, we would identify the model parameters that can be constrained robustly: for example, the quiescent time between bursts or the burst duration. Should our simple model fail to reproduce the observations we would learn, perhaps, at what mass scales, it would break down or if bursty star formation alone is not enough. To test

this idea we have built a simple parametric phenomenological model of bursty star formation (see Sec. 2) and compared its predictions to observations in the  $M_{UV}$  vs  $M_*$  plane, also known as the star formation main sequence (SFMS), in galaxies at  $z > 5$  (Sec 3). We will discuss the predicted luminosity function in Sec. 4 and draw our conclusions in Sec 5.

### 2. THE MODEL

In our toy model star formation happens in a series of instantaneous bursts labeled by the index  $i$ . The mass contributed by the  $i$ -th burst is a constant term plus a term proportional to the total stellar mass formed so far, namely:

$$\Delta M_i = \xi + \eta M_{i-1} \quad (1)$$

The bursts are separated by a time  $\Delta t$  which can be a constant or have a random dispersion. Unless otherwise stated we will use a constant  $\Delta t$ .

The first burst takes place after redshift  $z = 30$  in a time interval chosen randomly between 0 and  $10\Delta t$ . The random start time for the sequence of bursts for each galaxy ensures that different galaxies are not *in phase* and a spread of UV luminosities at a given  $M_*$  is observed. In practice, it also captures the diversity of halo masses at the initial redshift ( $z = 30$ ), simulating the fact that small-mass halos begin forming stars at later times than large-mass halos.

For the first burst,  $i=1$ ,  $M_0 = 0$  so  $\Delta M_1 = \xi$ . Therefore, the parameter  $\xi$  can be interpreted as the distribution of masses formed in the first burst. In labeling the models, we measure  $\xi$  in units of  $10^6 M_\odot$ .

Given that the elapsed time is proportional to the number of bursts (assuming constant  $\Delta t$ ), Equation (1) implies that the stellar mass in each galaxy increases linearly with time when  $\eta = 0$  and exponentially with time when  $\eta > 0$ . Therefore, the value of  $\eta$  describes a range of galaxies with different speeds of evolution for their stellar mass. Note that, as long as the interval between bursts is  $\Delta t \leq 100$  Myrs, the galaxy rest-frame UV luminosity is dominated by the intensity and elapsed time from the last burst.

Since at a given redshift galaxies have a range of masses, we run models in which  $\xi$  and  $\eta$  are random values generated between predefined extremes, and we assume constant  $\xi$  and  $\eta$  only to explore the effects of changing these parameters. For random values of  $\xi$ , we define a power-law slope  $\alpha_\xi$  and generate  $\xi$  uniformly for  $\alpha_\xi = 0$ , uniformly in  $\log \xi$  for  $\alpha_\xi = -1$  or uniformly in  $\xi^{(1+\alpha_\xi)}$  for  $\alpha_\xi \neq 0, -1$ . We can generate  $\eta$  in a similar way, keeping it constant or defining a coefficient  $\alpha_\eta$  that characterizes the random distribution. We list in Table 1 the basic properties of the subset of models that we discuss in the paper.

Galaxies evolve, burst after burst, until redshift 4 at which point the simulation ends. We define 21 sampling times uniformly spaced between redshift 12 and redshift 5 and "observe" each galaxy model at each of these times. For each "observation" we record the stellar mass and the 1500 Å rest frame UV luminosity computed from the contribution of each past burst weighted through the burst age vs luminosity relation from the low-metallicity model ( $Z = 0.002$ ) with Salpeter IMF in STARBURST99 (Leitherer et al. 1999).

The main comparison with JWST observations will be based on the  $M_{UV}$  vs stellar mass distribution at  $z > 5$ . We expected that at lower redshift other physical effects, such as continuous star formation, mergers,

In the figures and in our analysis, we consider redshift intervals containing the same number of "observations" and characterized by the same cosmic volume so that, after galaxies have had their first burst, the number of galaxies per cosmic volume remains constant. However, given that the first burst happens randomly in the time interval  $0 - 10\Delta t$  from  $z = 30$ , the number of galaxies is not strictly constant because some galaxies, not having experienced their first burst yet, are dark. Thus, aside from the presence of some dark galaxies (or galaxies below the detection limit), the evolution we see is effectively produced by the evolution of the luminosity

function rather than the evolution of the galaxy number density.

We have also explored the case where the first burst occurs randomly within the interval  $0 - \Delta t$  from  $z = 30$ , so that effectively all galaxies form stars from the beginning of the simulation (at  $z > 12$ ), giving a pure luminosity evolution as the total number of luminous galaxies between  $z=5$  and  $z=12$  is constant (e.g. Model 1ND in Table 1).

We can include an observability condition by requiring, e.g., that only objects with apparent AB magnitude brighter than some value  $m_{lim}$  are observable. In the following we adopt  $m_{lim} = 30$  in a narrow observer frame band located at the rest frame 1500 Å wavelength. Only objects brighter than this limit will be shown in the plots.

### 3. RESULTS

In this paper, we are focusing our comparison on  $M_{UV}$  vs stellar mass ( $M_*$ ) rather than the Star Formation Rate (SFR) vs  $M_*$ , as the former quantity is in principle directly observable and easily determined from the model. Star Formation Rate is usually determined by photometric fits that include multiple bands and it requires us to adopt a smoothing model for what would otherwise be the sum of delta-functions.

#### 3.1. Minimal Toy Models

First, we test minimal models in which  $\xi$ ,  $\eta$  and  $\Delta t$  are constant. These models are not realistic but we show them to illustrate the effects of varying each of the 3 free parameters in the model. For any choice of these parameters the models appear as a number of vertical lines in the  $M_{UV}$  vs  $M_*$  plane. Fig. 1 shows the distribution in our model (vertical lines) compared to the Morishita et al. (2024) sample of galaxies at  $z > 5$ .

Each vertical line, at a given mass, corresponds to a given number of bursts. A summary of the effects of varying each parameter while keeping the others constant is given below.

i) **Quiescence period  $\Delta t$ :** The vertical extent of the lines depends on  $\Delta t$ . Larger values of  $\Delta t$  introduce a larger luminosity scatter by enabling the most recent burst to age as much as  $\Delta t$ . Smaller  $\Delta t$  correspond to less aging and thus less dimming in the UV and, at the same time, galaxies with larger stellar mass as the number of bursts increases with decreasing  $\Delta t$ . The implications of this result is that for each choice of parameters we only see a relatively narrow range of discrete masses at each redshift. This is the main rationale for considering random distributions of  $\xi$  and/or  $\eta$ , in addition to

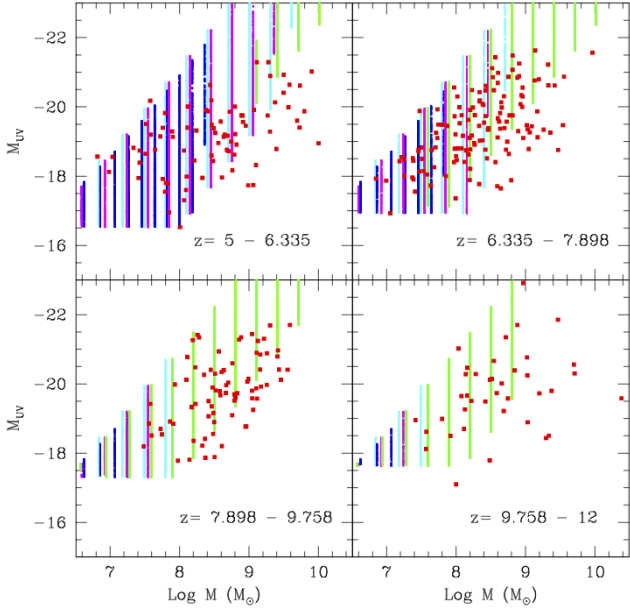


**Figure 1.** The cyan points show  $M_{UV}$  vs  $M_*$  for a model with  $\xi = 1$ ,  $\eta = 1$ , and  $\Delta t = 100\text{Myrs}$  (Model A in Table 1). Blue is for  $\xi = 1$ ,  $\eta = 0.5$  (Model B, displaced by -0.05 in log M for visibility purposes), and magenta for  $\xi = 0.5$  and  $\eta = 1$  (Model C, displaced by +0.05 in log M). Green is for with  $\xi = 1$ ,  $\eta = 1$ , and  $\Delta t = 50\text{Myrs}$  (Model D). We are only plotting models with apparent magnitude  $m_{UV} \leq 30$  to simulate an observational limit. Each vertical line corresponds to a given number of bursts and the number of bursts is related to redshift but is not a one-to-one function of redshift because of the random distribution of starting redshifts. The vertical extent of each line is related to the burst length  $\Delta t$ . The observational points in red are from Morishita et al. (2024).

also being a more physically motivated choice given the range of halo masses at any redshift.

ii) **Strength of first burst  $\xi$ :** Comparison of the model with the data in Fig. 1 shows that constant  $\xi$ ,  $\eta$  models do not seem to span the whole range of observed masses while also potentially over-predicting the observed luminosity. The latter effect is due to the fact that for  $\eta = 1$ , models with mass larger than  $10^8 \text{ M}_\odot$  can have extremely bright bursts exceeding  $10^8 \text{ M}_\odot$  of new stars.

iii) **Growth rate of the burst  $\eta$  :** Models with  $\eta = 0$  (linear mass growth rate) require values of  $\xi$  generally larger than in models with  $\eta > 0$ . However, both choices can be tuned to reproduce the range of  $M_*$  observed in the redshift range  $z = 5 - 12$ .

In all models the main challenge is to produce galaxies with the largest  $M_*$  without making too many overly bright galaxies (with  $M_{UV} < -22$ ). We will see that we found two solutions to this problem:

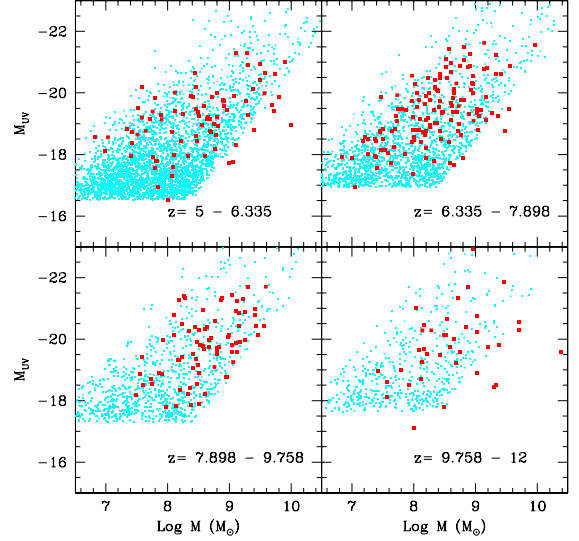


**Figure 2.**  $M_{UV}$  vs  $M_*$  for the galaxies in Morishita et al. (2024) compared to a model with a random distribution of  $\xi$  and  $\eta = 0$  as described in the text (Model 20 in Table 1). The redshift bins in each panel have the same cosmic volume.

1) Increasing the duration of each burst. This allows each burst to produce a large mass in stars without making overly luminous galaxies in the rest-frame UV, as the formation of short-lived massive stars is spread over a time larger than their life on the main sequence, setting a maximum limit to their instantaneous number.

2) Assuming a distribution for  $\xi$  that makes the number of galaxies producing large bursts in stars relatively rare, hence more unlikely to be observed at their peak luminosity. Nevertheless these galaxies exist, grow to have a large stellar mass, but are typically observed at fainter UV brightness than at their peak luminosity (i.e., after a major burst of star formation).

### 3.2. More realistic models

On the basis of the inadequacy of models with constant  $\xi$  and  $\eta$ , let's consider now a model where  $\eta = 0$ ,  $\Delta t = 100 \text{ Myrs}$ , and where  $\xi$ , i.e. the mass-independent strength of a burst, is randomly assigned to each galaxy with a uniform power-law distribution with slope  $\alpha_\xi = -1.8$  and with  $\xi_{min} = 1$  and  $\xi_{max} = 5000$ . The resulting distribution is given in Fig. 2 (see also Model 20 in Table 1). This particular model seems to reproduce the observed distribution at all redshift. Models with lower values of  $\xi_{max}$ , as e.g. Model 1 in Table 1) are unable to produce the high masses seen at  $z > 10$ .

Assuming constant  $\xi = 1$  and a random  $\eta$  uniformly extracted in, e.g., the range 0.01-3 we would obtain very high luminosities due to very intense bursts (Model 9M in Table 1). To maintain the match with observations we need to effectively increase the duration of each burst.

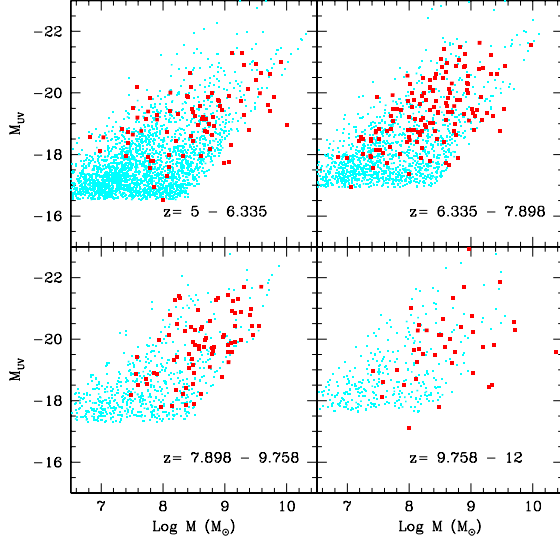


**Figure 3.**  $M_{UV}$  vs  $M_{\star}$  for the galaxies in Morishita et al. (2024) compared to a model with  $\eta = 0$  and  $\xi$  randomly distributed with  $\alpha_{\xi} = -2$ . Details are described in the text (Model 19 in Table 1). The slope of luminosity function for this model is compatible with the observed one.

We do this, within our simple scheme, by introducing a maximum instantaneous burst mass. Essentially, we split the desired burst into multiple smaller bursts occurring one after the other with a 5 Myrs separation. This was not needed for the model above because the overall probability of intense bursts was lower.

We also consider models where both  $\xi$  and  $\eta$  are randomly distributed with  $\alpha_{\xi} = -1.5$  and  $\alpha_{\eta} = -1.5$  (e.g. Model 5 in Table 1). Even these models can reproduce the range of masses and luminosities that are observed but tend to under-predict the most luminous objects at  $z \geq 8$  unless  $\xi_{max} > 1000$ . Thus, considering  $\eta \neq 0$  does not allow us to avoid large values of  $\xi_{max}$ .

We have verified that the results discussed above would not change if the interburst spacing  $\Delta t$  was given a random dispersion instead of being fixed to a given value.

#### 4. LUMINOSITY FUNCTION SLOPE

From our models we can derive the luminosity function (LF) at different redshifts. For models where  $\eta$  is a constant and  $\xi$  is a random power-law distribution with slope  $\alpha_{\xi}$ , naively we expect a slope of the LF as a function of luminosity identical to the slope in  $\xi$ : i.e.,  $\alpha_{LF} = \alpha_{\xi}$ . Therefore the LF slope as a function of UV magnitude is  $\alpha_{LF,mag} = 0.4(\alpha_{\xi} + 1)$ , obtained converting from luminosity to magnitude distributions. In Fig. 4 we show the LF for a model with  $\eta = 0$  and a random distribution of  $\xi$  with slope  $\alpha_{\xi} = -1.5$  (aka Model 1). No magnitude cutoff has been applied here

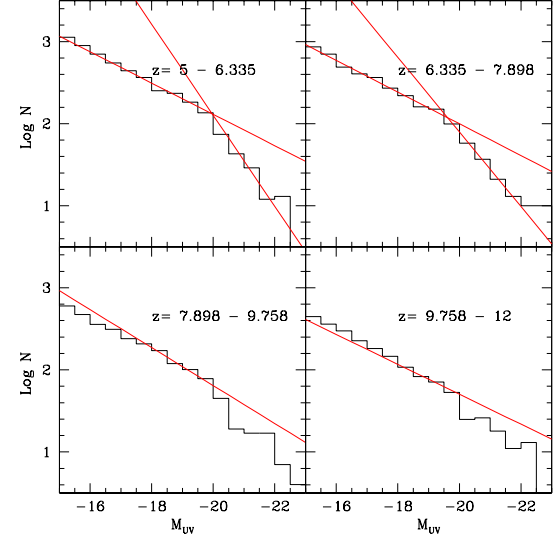


**Figure 4.** log counts vs  $M_{UV}$  for the models with  $\eta = 0$  and a random power-law distribution of  $\xi$  (Model 1). The slope break around  $M_{UV} \simeq -21$  is due to the adopted  $\Delta t = 0.1$  and the dimming of a burst over the time  $\Delta t$ . The red lines show a broken power law fit to the LF with  $\alpha_{faint} = -0.2$  and  $\alpha_{bright} = -0.5$  at  $z = 5 - 6$ ,  $\alpha_{faint} = -0.19$  and  $\alpha_{bright} = -0.27$  at  $z = 6 - 8$ , and  $\alpha_{faint} = -0.2$  at higher  $z$ .

to allow for a better fit. We find that the faint end slope  $\alpha_{LF,mag} \approx -0.2$  of the LF agrees with the slope predicted above (dictated by the slope imposed for  $\xi$ ,  $\alpha_{\xi} = -1.5$ ).

At redshifts  $z < 8$  the LF is well described by a broken power-law, even though our  $\xi$  distribution is a single power-law with slope that matches the faint-end of the LF. The slope of the power-law at the bright end is steeper than at the faint end. We explain this effect as produced by the duty cycle of the bursts in the rest-frame UV: the number of galaxies that are observed at a given UV luminosity is proportional to the fraction of time they spend at that given luminosity (i.e., the duty cycle). Since, for an instantaneous burst, the UV luminosity drops very rapidly with elapsed time from the burst, the time spent at the peak luminosity is short, while the time spent at fainter luminosity is longer. Therefore, the number of bright galaxies is suppressed more strongly than the number of faint galaxies, producing a steeper drop at the bright end when compared to the input power-law of the bursts. In other words, the break is not caused by the assumed burst distribution but by the fact that a burst can be randomly observed at maximum brightness or after a time  $\Delta t$  has elapsed (i.e. just before the next burst occurs). Reducing the value of  $\Delta t$  moves the break to brighter magnitudes, and vice-versa.

It is interesting that this broken power law behavior is unrelated to the exponential cut off of the dark matter halos mass function (which we do not consider here) but it's simply due to the imposed burst strength power-law and the dimming due to the inter-burst spacing. Note that in our model the break between the two power-laws is independent of redshift as long as the inter-burst spacing is also independent of redshift.

In order to reproduce the observed luminosity function  $\alpha_{LF} \simeq -2$  we need  $\alpha_\xi \simeq -2$ . For such slopes the break discussed above is not readily visible.

#### 4.1. Minimal model that fits the data

It turns out that the model that best fits the data is also the simplest. This is Model 19, which has linear growth  $\eta = 0$ , burst spacing  $\Delta t = 100$  Myr, and a power-law distribution for  $\xi$  in the range  $1 < \xi < 10^4$  with slope -2 (see Fig. 3).

We note that the distribution of stellar masses at  $z > 10$  roughly represents the distribution of initial masses  $\xi$  of the first burst. Hence, we chose a  $\xi$  that fits the high- $z$  galaxies. Since the of the observed stellar masses do not increase substantially from redshift  $z \sim 10$  to  $z \sim 5$ , a model with galaxies having exponential growth of their stellar mass does not match the data.

It is worth noting that cosmological zoom-in simulations of galaxies at  $z > 8$ , in which the resolution is sufficient to resolve the formation of compact star cluster, show a bursty SF with  $\Delta t \sim 100$  Myr and roughly equal strength of repeated starburst (Garcia et al. 2025), in good agreement with our minimal model.

## 5. DISCUSSION AND CONCLUSIONS

We find that a simple toy model where we assign to each galaxy two burst parameters and define a burst time separation for all objects can reproduce the distribution of galaxies in the Mass-UV luminosity plane at  $z \geq 5$ . In addition the model the best reproduces the observation is even simpler: it has a linear growth of the stellar mass in each galaxy ( $\eta = 0$ ) and a constant time between bursts of 100 Myr.

Below is a summary of our findings:

- Given these assumptions, the model that best reproduces the observations has a linear growth of the stellar mass in each galaxy ( $\eta = 0$ ) and a constant time between bursts of 100 Myr.

- The distribution of initial masses of the galaxies (during their first burst) is a power law with slope  $\alpha_\xi \sim -2$ , within a minimum and maximum mass of  $(10^6, 10^{10}) M_\odot$ . This distribution also represents the distribution of stellar masses of observed galaxies at  $z > 10$ . The largest stellar mass at these redshift is  $M_* \sim 10^{10} M_\odot$ . This is a large value but not physically unrealistic for dark matter halos of mass  $M \sim 10^{11} - 10^{12} M_\odot$ , which are rare at  $z > 10$ . Here we take a purely empirical approach, and we do not speculate on whether it is possible to form these many stars in a single burst of star formation. Several previous papers (Dekel et al. 2023; Ferrara 2024; Andalman et al. 2025) have proposed mechanisms that may be at play in the high redshift universe that may facilitate such large starbursts.
- The galaxy luminosity function at high redshift appears well fitted by a double power law (e.g. Donnan et al. 2024) while our models reproducing naturally the faint end slope do now show such feature. In contrast, our models with shallower faint-end slope display a steeper slope at high luminosity - but not as steep as observed - due to burst aging effects. The inability of our model to reproduce the steep bright end slopes could be due to the fact that we do not incorporate possible effects related to the exponential cut off in the number density of massive halos in the halo mass function, or other effects related to burst duration and aging, or changes in the IMF in brighter galaxies. Exploring this effect further goes beyond the purpose of this paper.

<sup>1</sup> We thank the anonymous referee for comments that helped improved the paper. MS acknowledges the hospitality of the University of Maryland - College Park during the preparation of this paper as well as support for this work under NASA grant 80NSSC22K1294.

## REFERENCES

**Table 1.** Summary of model properties

ID	$\xi$	$\eta$	$\Delta t$ (Myrs)	1st burst	Burst	Model vs Data			Notes
				delay (in $\Delta t$ )	splitting	$[M_* @ z > 9.76]$	$[M_{UV} < -22]$	Verdict	
A	1	1	100	10	N	87%	45%	$\times/\times$	exp. SF
B	1	0.5	100	10	N	95%	6%	$\times/\checkmark$	
C	0.5	1	100	10	N	94%	39%	$\times/\times$	dep. on $\xi$
D	1	1	50	10	N	57%	48%	$\times/\times$	dep. on $\Delta t$
E	1	0	100	10	N	100%	0%	$\times/\checkmark$	uniform SF
1	(0.17,480,-1.5)	0	100	10	N	32%	18%	$\times/\checkmark$	
1ND	(0.17,480,-1.5)	0	100	1	N	24%	12%	$\checkmark/\checkmark$	LF too flat
5	(0.17,480,-1.5)	(0,3,-1.5)	100	10	N	28%	47%	$\checkmark/\times$	
8	(0.17, 480, -1.5)	1	100	10	N	24%	52%	$\checkmark/\times$	
8M	(0.17, 480, -1.5)	1	100	10	Y	46%	7%	$\times/\checkmark$	
9M	1	(0,3,0)	100	10	Y	73%	6%	$\times/\checkmark$	
10	(0.17,480,-1.5)	(0, 3, 0)	100	10	N	21%	55%	$\checkmark/\times$	
11	(0.17,2000,-1.5)	0	100	10	N	20%	29%	$\checkmark/\checkmark$	LF too flat
12	(0.17,2000,-1.8)	0	100	10	N	40%	25%	$\times/\checkmark$	
13	(0.17,5000,-1.8)	0	100	10	N	37%	30%	$\times/\times$	
18	(0.17,10000,-2)	0	100	10	N	62%	9%	$\times/\checkmark$	
19	(1,10000,-2)	0	100	10	N	28%	21%	$\checkmark/\checkmark$	best model
20	(1,5000,-1.8)	0	100	10	N	21%	28%	$\checkmark/\checkmark$	good

NOTE— A more detailed description of the parameters is in the text. In the  $\xi$  and  $\eta$  columns we either give one value or three. When one value is given, the parameter is kept constant at that value. When three are given, the parameter is varied between the first two values using a power-law slope given by the third value. When burst splitting is enabled we split any burst creating more than  $60M M_\odot$  into multiple bursts separated by 5 Myrs.

Caputi, K. I., Rinaldi, P., Iani, E., et al. 2024, ApJ, 969, 159, doi: [10.3847/1538-4357/ad4eb2](https://doi.org/10.3847/1538-4357/ad4eb2)

Dekel, A., Sarkar, K. C., Birnboim, Y., Mandelker, N., & Li, Z. 2023, MNRAS, 523, 3201, doi: [10.1093/mnras/stad1557](https://doi.org/10.1093/mnras/stad1557)

Donnan, C. T., McLure, R. J., Dunlop, J. S., et al. 2024, MNRAS, 533, 3222, doi: [10.1093/mnras/stae2037](https://doi.org/10.1093/mnras/stae2037)

Ferrara, A. 2024, A&A, 684, A207, doi: [10.1051/0004-6361/202348321](https://doi.org/10.1051/0004-6361/202348321)

Garcia, F. A. B., Ricotti, M., & Sugimura, K. 2025, arXiv e-prints, arXiv:2503.08779, doi: [10.48550/arXiv.2503.08779](https://doi.org/10.48550/arXiv.2503.08779)

Leitherer, C., Schaerer, D., Goldader, J. D., et al. 1999, ApJS, 123, 3, doi: [10.1086/313233](https://doi.org/10.1086/313233)

Morishita, T., Stiavelli, M., Chary, R.-R., et al. 2024, ApJ, 963, 9, doi: [10.3847/1538-4357/ad1404](https://doi.org/10.3847/1538-4357/ad1404)

Pallottini, A., Ferrara, A., Gallerani, S., et al. 2024, arXiv e-prints, arXiv:2408.00061, doi: [10.48550/arXiv.2408.00061](https://doi.org/10.48550/arXiv.2408.00061)

Rinaldi, P., Navarro-Carrera, R., Caputi, K. I., et al. 2024, arXiv e-prints, arXiv:2406.13554, doi: [10.48550/arXiv.2406.13554](https://doi.org/10.48550/arXiv.2406.13554)

Sugimura, K., Ricotti, M., Park, J., Garcia, F. A. B., & Yajima, H. 2024, ApJ, 970, 14, doi: [10.3847/1538-4357/ad499a](https://doi.org/10.3847/1538-4357/ad499a)